doi:10.1093/brain/awq336 Brain 2011: 134; 585–601 | 585

BRAIN
A JOURNAL OF NEUROLOGY

$Na_v1.8$ channelopathy in mutant mice deficient for myelin protein zero is detrimental to motor axons

Mihai Moldovan,[1,2] Susana Alvarez,[1,2] Volodymyr Pinchenko,[1] Dennis Klein,[3] Finn Cilius Nielsen,[4] John N. Wood,[5] Rudolf Martini[3,*] and Christian Krarup[1,2,*]

1 Institute of Neuroscience and Pharmacology, Panum, University of Copenhagen, Denmark
2 Clinical Neurophysiology, Rigshospitalet, Copenhagen, Denmark
3 Department of Neurology, Developmental Neurobiology, University of Würzburg, Germany
4 Department of Clinical Biochemistry, Rigshospitalet, University of Copenhagen, Denmark
5 Molecular Nociception Group, University College London, London, UK

*Shared senior authorship

Correspondence to: Prof. C. Krarup, MD DMSc FRCP,
Department of Clinical Neurophysiology NF3063,
Rigshospitalet,
9 Blegdamsvej,
2100 Copenhagen,
Denmark
E-mail: ckrarup@rh.dk

Myelin protein zero mutations were found to produce Charcot–Marie–Tooth disease phenotypes with various degrees of myelin impairment and axonal loss, ranging from the mild 'demyelinating' adult form to severe and early onset forms. Protein zero deficient homozygous mice ($P_0^{-/-}$) show a severe and progressive dysmyelinating neuropathy from birth with compromised myelin compaction, hypomyelination and distal axonal degeneration. A previous study using immunofluorescence showed that motor nerves deficient of myelin protein zero upregulate the $Na_V1.8$ voltage gated sodium channel isoform, which is normally present only in restricted populations of sensory axons. The aim of this study was to investigate the function of motor axons in protein zero-deficient mice with particular emphasis on ectopic $Na_V1.8$ voltage gated sodium channel. We combined 'threshold tracking' excitability studies with conventional nerve conduction studies, behavioural studies using rotor-rod measurements, and histological measures to assess membrane dysfunction and its progression in protein zero deficient homozygous mutants as compared with age-matched wild-type controls. The involvement of $Na_V1.8$ was investigated by pharmacologic block using the subtype-selective $Na_V1.8$ blocker A-803467 and chronically in $Na_V1.8$ knock-outs. We found that in the context of dysmyelination, abnormal potassium ion currents and membrane depolarization, the ectopic $Na_V1.8$ channels further impair the motor axon excitability in protein zero deficient homozygous mutants to an extent that precipitates conduction failure in severely affected axons. Our data suggest that a $Na_V1.8$ channelopathy contributed to the poor motor function of protein zero deficient homozygous mutants, and that the conduction failure was associated with partially reversible reduction of the electrically evoked muscle response and of the clinical function as indicated by the partial recovery of function at rotor-rod measurements. As a consequence of these findings of partially reversible dysfunction, we propose that the $Na_V1.8$ voltage gated sodium channel should be considered as a novel therapeutic target for Charcot–Marie–Tooth disease.

Keywords: nerve activity; regeneration; ion channels; excitability; node of Ranvier, internode

Abbreviations: CMAP = compound muscle action potential; P_0 = myelin protein zero; SNS = slowly inactivating, tetrodotoxin resistant $Na_v1.8$ voltage gated sodium channel isoform

Received May 15, 2010. Revised October 13, 2010. Accepted October 14, 2010. Advance Access publication December 17, 2010

Introduction

The extracellular leaflets of peripheral nervous system myelin are held together by the homophilic interactions of the extracellular domains of myelin protein zero (known as MPZ or P_0), a 28 kDa single pass transmembrane glycoprotein of the immunoglobulin superfamily. (Filbin *et al*., 1990; Lemke, 1993; Shapiro *et al*., 1996). Apart from its role in myelin compaction, P_0 was also found to be involved in the spiralling process leading to myelin formation, determination of the appropriate myelin thickness, and ultimately the maintenance of the myelin sheeth and axons (Martini and Schachner, 1997).

The human P_0 gene is located on chromosome 1 and is one of the identified causative genes in the hereditary motor and sensory peripheral neuropathy known as Charcot–Marie–Tooth disease that is typically associated with muscular weakness and atrophy, sensory dysfunction and skeletal deformities. P_0 mutations were found to produce Charcot–Marie–Tooth disease phenotypes with varying degrees of myelin impairment and axonal loss, ranging from the mild 'demyelinating' adult forms to particularly severe and early onset forms (Warner *et al.*, 1996; Wrabetz *et al.*, 2006; Reilly and Shy, 2009). Furthermore, some P_0 mutations were even found to cause loss of axons in the absence of demyelination (Marrosu *et al.*, 1998; Li *et al.*, 2006). Thus, it is likely that P_0 mutations can cause both 'loss of function' and 'gain of function' pathologies leading to axonal degeneration, which represents the final common pathway of all Charcot–Marie–Tooth disease subtypes (Nave *et al.*, 2007). To date there are no effective treatments for Charcot–Marie–Tooth disease in humans.

P_0 deficient homozygous ($P_0^{-/-}$) mice show a severe and progressive dysmyelinating neuropathy from birth with compromised myelin compaction, hypomyelination and distal axonal degeneration (Frei *et al.*, 1999; Samsam *et al.*, 2003; Ey *et al.*, 2007). A previous immunofluorescence study (Ulzheimer *et al.*, 2004) revealed that in $P_0^{-/-}$ mice the myelin alteration was associated with a profound disruption of the axonal membrane architecture with immature nodal clusters of voltage gated sodium channels and disorganization of paranodal and juxtaparanodal K^+ channels. Most strikingly, P_0-deficient motor nerves displayed ectopic expression of the $Na_V1.8$ isoform (Ulzheimer *et al.*, 2004). This is particularly intriguing as in the peripheral myelinated motor axons, conduction at nodes of Ranvier is typically ensured only by the fast inactivating tetrodotoxin-sensitive $Na_V1.6$ voltage-gated Na^+ channel isoform (Goldin *et al.*, 2000; Krzemien *et al.*, 2000; Novakovic *et al.*, 2001). In contrast, the slowly inactivating, tetrodotoxin-resistant $Na_v1.8$ voltage gated sodium channel isoform (SNS) is typically expressed in unmyelinated sensory neurons (C-fibres) (Akopian *et al.*, 1996, 1999; Kozak and Sangameswaran, 1996; Novakovic *et al.*, 2001). The pathophysiological implication of $Na_V1.8$ co-expression with $Na_v1.6$ in the P_0-deficient mouse mutant is unclear but raises the possibility that a 'voltage gated sodium channels channelopathy' may contribute to the poor motor function in these mutants.

The aim of this study was to investigate the function of motor axons in P_0 deficient mice with particular emphasis on ectopic $Na_V1.8$ voltage gated sodium channels. The only electrophysiological method that can be used to study the membrane ion channel function of undissected peripheral motor axons is nerve excitability testing by automatically tracking the changes in 'threshold current' required to evoke a submaximal target compound muscle action potential (CMAP) (Bostock *et al.*, 1998; Kiernan *et al.*, 2000). Recently, such nerve excitability methods were adapted to study mouse motor axons (Moldovan and Krarup, 2006; Nakata *et al.*, 2008; Sawai *et al.*, 2008; Boerio *et al.*, 2009, 2010; Moldovan *et al.*, 2009*a*).

We combined 'threshold tracking' excitability studies with conventional nerve conduction studies, behavioural studies and histological and immunohistochemistry measures to assess membrane dysfunction and its progression in $P_0^{-/-}$ mutants as compared with age-matched wild-type controls. The involvement of $Na_V1.8$ was investigated by pharmacological blocking using the subtype-selective $Na_V1.8$ blocker A-803467 (Jarvis *et al.*, 2007) and chronically in $Na_V1.8$ knock-outs (Akopian *et al.*, 1999).

Brief preliminary reports have been published (Moldovan *et al.*, 2008, 2009*b*).

Materials and methods

Animals and experimental design

In Copenhagen we established our own colony of P_0 deficient mice (Giese *et al.*, 1992) backcrossed on C57Bl6 mice using breeding pairs from the original colony in Würzburg (Schmid *et al.*, 2000). DNA was extracted from tail clips with the Qiagen DNeasy Blood and Tissue Kit (Copenhagen, Denmark). Genotyping of P_0-mutants was carried out by a conventional polymerase chain reaction employing primers 5′-TCAGTTCCTTGTCCCCCGCTCTC-3′, 5′-GGCTGCAGGGTCGCTCG GTGTTC-3′, and 5′-ACTTGTCTCTTCTGGGTAATCAA-3′ (Sigma-Aldrich Denmark A/S, Brøndby, DK) generating amplicons of 334 or 500 bp for the P_0 null mutation and wild-type allele, respectively (Schmid *et al.*, 2000).

Mice deficient for $Na_V1.8$ were generated by targeting the S4 voltage sensor of domain I of the SNS Na^+ channel α subunit as previously described (Akopian *et al.*, 1999). The null mutants expressing a non-functional SNS transcript were healthy and fertile. Mice deficient for both P_0 and $Na_V1.8$ were generated by crossing P_0 heterozygotes with SNS null mutants backcrossed onto C57Bl6 mice obtained from the original colony at University College London, UK (Akopian *et al.*, 1999). Genotypes of the SNS mice were verified by conventional polymerase chain reaction using oligonucleotides 5′-GACTGATGCAT ATGATGTCATGTGTGG-3′, 5′-GCCTTCACTGTTGTTTACACCTCCGA GG-3′ and 5′-GCAGCGCATCGCCTTCTATC-3′ (Sigma-Aldrich Denmark A/S) leading to amplicons of 900 or 1100 bp for the SNS null mutation and wild-type allele, respectively. P_0-deficiency in the double mutants was tested by conventional polymerase chain reaction as described above.

Experiments were carried out over three years in 127 mice: 42 wild-type, 59 homozygously deficient for P_0 ($P_0^{-/-}$), 12 homozygously deficient for $Na_V1.8$ ($SNS^{-/-}$) and 14 homozygously deficient for both P_0 and $Na_V1.8$ ($P_0SNS^{-/-}$). *In vivo* electrophysiological studies under anaesthesia and behavioural measurements of motor performance were only carried out in $P_0^{-/-}$ mutants up to five months of age because of the severe disease course in these mice. At the completion of the experiments all the mice were killed by cervical dislocation.

Experimental procedures were approved by the Danish National Animal Experiment Committee.

Electrophysiological investigations of the tibial nerve under anaesthesia

For anaesthesia a 1:1 mixture of hypnorm/midazolam (5 mg/ml) was used instead of isoflurane, which can affect $Na_V1.8$ currents (Herold *et al.*, 2009). A volume of 0.1 ml/10 g from the mixture was injected subcutaneously for induction, and then maintained with 50% hourly for up to 4 h as needed.

The anaesthetized mouse was fixed in a stereotaxic frame (dual manipulator with mouse adaptor 51624, Stoelting) on a temperature controlled pad (HB 101/2, LSI Letica) set to 37°C. The investigated leg was placed on a piece of hydrophobic cotton and clamped from the distal toes as previously described (Moldovan *et al.*, 2009*a*).

Electrical stimuli were delivered from a constant current stimulator (DS4, Digitimer Ltd) to the tibial nerve via custom-made platinum needle electrodes. The cathode was inserted at the ankle and the anode was inserted at the base of the tail. The evoked CMAP was recorded from plantar muscles using needle electrodes inserted into the foot ~0.5 cm apart. A ground electrode was inserted subcutaneously between stimulation and recording electrodes.

The amplified signal (10 Hz–6 kHz, 10C02, Dantec) was digitized by computer (PC) with an analogue-to-digital (A/D) board (NI-6221, National Instruments Inc.) at a sampling rate of 10 kHz. CMAP amplitudes were measured peak-to-peak. Latencies of the fastest conducting axons were measured to the first deviation from baseline.

In selected cases, tibial nerve studies were supplemented with electromyographical (EMG) examination of spontaneous activity of the anterior tibial muscle using concentric needle electrodes.

Multiple measures of tibial nerve excitability

Peripheral nerve excitability was assessed using QtracS stimulation software (Institute of Neurology, London, UK). First, the stimulus-response curves were obtained using test stimuli of 1 ms duration to establish the maximal CMAP (100%) to supramaximal nerve stimulation and corresponding stimulus-response slope calculated as [(stimulus for 75% CMAP)-(stimulus for 25% CMAP)]/(stimulus for 50% CMAP). Then, the 'threshold' current necessary to evoke a submaximal target potential set to 40% of maximum CMAP could be automatically tracked by trial-and-error computer feedback optimized on stimulus-response slope.

Although threshold is a global index of excitability (i.e. an increase in threshold corresponds to a decrease in excitability), the absolute value of threshold yields little information about the underlying membrane function (Bostock *et al.*, 1998). Instead, relative changes in threshold in various experimental settings were determined using the TRONDH (K-N) multiple excitability sequence as previously described (Bostock *et al.*, 1998; Kiernan *et al.*, 2000; Tomlinson *et al.*, 2010): (i) strength–duration relationship; (ii) threshold electrotonus; (iii) current–threshold relationship and (iv) recovery cycle.

The strength–duration properties reflecting primarily the function of nodal membrane (Mogyoros *et al.*, 1996, 2000) were determined by measuring the changes in thresholds for test stimuli of 0.2, 0.4, 0.6, 0.8 and 1.0 ms duration. Rheobase and the strength–duration time constant were estimated from the corresponding linear charge (current strength × duration) – duration relationship using Weiss's law (Bostock, 1983): rheobase from the slope and strength–duration time constant from the negative intercept on the duration axis. The contribution of Na^+ currents to strength–duration time constant was further investigated using a latent addition (LA) protocol as previously described (Bostock and Rothwell, 1997; Nakata *et al.*, 2008). Briefly, the decay of the threshold increase following a strong hyperpolarizing stimulus (90% of threshold) is the sum of two exponentials corresponding to the passive (fast) and active components (slow) time constants. After 0.2 ms following the stimulus, the threshold is primarily determined by the slow component that was quantified as LAh (0.2 ms).

Paranodal-internodal membrane function was ascertained by investigating changes in threshold in response to prolonged depolarization/hyperpolarization comprised in threshold electrotonus and current–threshold relationship. Threshold electrotonus (TE) was measured for 100 ms depolarizing and hyperpolarizing polarizing currents set to 40% of the control threshold current. The maximal threshold change during depolarization was quantified as the mean threshold reduction between 10 and 20 ms referred to as TEd(10–20 ms). The subsequent plateau value reached within 100 ms was quantified as TEd(90–100 ms). Hence, the membrane accommodation to depolarization could be quantified as the difference between TEd(10–20 ms) and TEd(90–100ms) and the corresponding accommodation half-time could be determined. By analogy, TEh(20–40 ms) and TEh(90–100ms) were quantified during hyperpolarization. Membrane accommodation to hyperpolarization was quantified as the difference between TEh(20–40 ms) and TEh(90–100 ms). However, threshold changes during hyperpolarization do not accommodate to plateau within 100 ms. Excitability changes after 200 ms current pulses from 50 to −100% in 10% steps were tested during current–threshold relationship, a threshold analogue of I/V relationship. Apart from providing TEh(200 ms), current-threshold relationship was used to calculate the minimum I/V slope (a threshold analogue for the passive input conductance) by fitting a straight line through each adjacent three points in turn.

Changes in threshold following a single supramaximal stimulus (RC1) were tested at 19 intervals from 1.5–200 ms during recovery cycle. Refractoriness during the relative refractory period was measured as threshold increase at 2 ms. Further fluctuations in recovery cycle were measured as superexcitability (the minimum mean of three adjacent points on the recovery cycle) and subexcitability (the maximum mean of three adjacent points after 10 ms).

Methodological considerations on using platinum electrode for excitability testing in mice

Stimulation via Pt needles inserted close to the tibial nerve at ankle requires less current than stimulation via surface Ag/AgCl electrodes, which is particularly important for recording the strength-duration properties and recovery cycle in demyelinated mouse nerves with high thresholds (Moldovan and Krarup, 2006; Moldovan *et al.*, 2009*a*). Nevertheless, a potential source of error using Pt needle electrodes as compared with Ag/AgCl electrodes is their susceptibility to polarization that might alter the threshold deviations during electrotonus and current-threshold relationships. In a previous study using a custom-made stimulator, we found that the difference between Pt needle electrodes and surface Ag/AgCl electrodes was negligible at the low currents required for stimulating mouse motor axons (Moldovan *et al.*, 2009*a*). Here we confirmed our observations in both wild-type and P_0 using the DS4 commercially available stimulator in a set of control experiments (data not shown). Furthermore, the

magnitude of threshold deviations during threshold electrotonus and current-threshold relationships obtained here with Pt needles in wild-type were similar to those reported with Ag/AgCl surface electrodes in mouse tibial nerves (Boerio *et al.*, 2009, 2010).

Pharmacological $Na_V1.8$ block

The subtype-selective $Na_V1.8$ blocker 5-(4-chlorophenyl)-N-(3,5-dimethoxyphenyl) furan-2-carboxamide (A-803467), originally developed by Abbott Laboratories (Jarvis *et al.*, 2007), was obtained from Sigma-Aldrich (Denmark A/S, Brøndby, DK). A-803467 was dissolved in polyethylene glycol (PEG 400, Sigma-Aldrich). For complete solution, addition of dimethyl sulphoxide solvent (DMSO, Sigma-Aldrich) was required. Care was taken to limit dimethyl sulphoxide to a few drops (1–2% of volume) to avoid potential cardiac side-effects in mice (Kramer *et al.*, 1995). This was further verified by continuous electrocardiographic recordings in control experiments using a Biopac MP150 data acquisition system (Biopac. Systems Inc., CA, USA) (data not shown).

A-803467 was prepared in concentrations up to 100 mg/kg for administration in a 0.1 ml/10 g subcutaneous injection.

Motor performance

Estimation of motor performance was performed using an accelerating Rota-Rod (Ugo Basile Srl, 21025 Comerio VA, Italy). After the mice were placed on the rod, the counter was started and the rod was accelerated from 4 to 40 rpm (Hockly *et al.*, 2003) over a period of 300 s. Any mice remaining on the apparatus after 600 s were removed and the rotor rod time scored as 600. Each determination represents the longest endurance time of three consecutive measurements repeated at 10 min intervals.

Morphological studies

At completion of the experiments, tibial nerves were removed and fixed by immersion in glutaraldehyde (2.0% in 0.1 M cacodylate buffer) for 24 h. The fixed nerves were post-fixed in 1% osmium tetroxide in 0.1 M Sørensen's buffer, dehydrated in graded alcohol (30 − 100%), cleared in propylene oxide and embedded in increasing concentrations of epoxy resin until polymerized in pure Epon™ in a heated cabinet. Cross sections of the tibial nerve at the ankle (corresponding to the electrophysiological stimulation site) were cut with dry glass knives at 2–3 μm, overstained with P-phenylenediamine, mounted and investigated with a light microscope (Olympus BX51, Olympus Danmark A/S, Ballerup, Denmark).

Overview micrographs (×40/0.90 UplanSApo Olympus objective) and detail micrographs (×100/1.40 Oil UplanSApo Olympus objective) were photographed with a digital camera (Olympus DP71) at 9 pixels/μm and 23 pixels/μm, respectively by the Visiopharm Integrator system (Visiopharm A/S, Hoersholm, Denmark).

Digital images were processed using the MNERVE custom-made nerve morphometry software developed in MATLAB (version 2010a, MathWorks, Inc., Natick, MA, USA). First, the total nerve area was traced from the overview micrographs. Then detail micrographs (at least 10% of the total nerve area) were used to automatically trace the 'myelin rings'. Axonal diameter and fibre diameter were calculated as the diameter of the circle having the same area as the inner contours and outer contours of the 'myelin rings', respectively. Average myelin thickness could then be calculated as half of the difference between the calculated axonal diameter and fibre diameter. Incomplete myelin rings (i.e. at the border of the measured region) were only counted.

The fibre density within the measured area was then used to calculate the total number of myelinated axons. In dysmyelinated P_0 nerves, such light microscopy counts include both the abnormally myelinated axons and the out-sorted larger axons devoid of myelin (promyelinated axons).

Immunohistochemistry

Teased fibre preparations of femoral quadriceps nerves from 4–5 month-old wild-type ($n = 3$), $P_0^{-/-}$ ($n = 3$) and $P_0SNS^{-/-}$ ($n = 4$) mice were prepared to examine the distribution of K_v channels ($K_v1.2$) by immunohistochemistry, as previously described (Ulzheimer *et al.*, 2004). Expression of Kv channels was quantified by the categories 'juxta-paranodal', 'asymmetric' and 'missing', in comparison to the paranodal marker Caspr. Between 85 and 100 nodes of Ranvier were examined per mouse.

Data analysis

Results in numbers are given as mean ± S.E.M. Plotting and statistical comparison of multiple measures nerve excitability was carried out using QtracP software (Institute of Neurology). Other comparisons were carried out using SPSS (Statistical Package for the Social Sciences version 17, SPSS, Inc.). The statistical test and level of significance is mentioned where used and levels of <0.05 were considered significant.

Results

Conduction and excitability abnormalities in myelin protein zero deficient mice

When compared with wild-type, even at age 1–2 months, $P_0^{-/-}$ mice had severely impaired CMAPs with prolonged latency from 0.96 ± 0.03 ms to 3.84 ± 0.08 ms (Mann–Whitney $P < 0.01$, Fig. 1A) and reduced amplitudes from 6.8 ± 0.4 to 0.4 ± 0.04 mV (Mann–Whitney $P < 0.01$, Fig. 1A). EMG recordings in $P_0^{-/-}$ mice showed not only denervation activity but also spontaneous repetitive discharges ($n = 3$, data not shown) in agreement with previous reports (Zielasek *et al.*, 2000).

Threshold tracking could be reliably performed in $P_0^{-/-}$ mice although tracking error was larger in severely affected nerves, and only CMAPs above 0.1 mV were included.

In $P_0^{-/-}$ mice there was overall reduction in excitability, measured as an increase in strength-duration rheobase to 0.5 ± 0.1 mA as compared with 0.1 ± 0.1 mA in wild-type (Mann–Whitney $P < 0.01$). The corresponding strength–duration time constant was however markedly increased to 691 ± 70 μs (Mann–Whitney $P < 0.01$) as compared with 177 ± 37 μs in wild-type mice (Fig. 2A).

The alterations in strength-duration properties occurred in the context of a marked threshold deviation during hyperpolarizing electrotonus measured as a change in TEh(20–40 ms) by 146% of threshold (from -84 ± 2 to -230 ± 14% Fig. 2B, Mann–Whitney $P < 0.01$) in spite of pronounced accommodation to hyperpolarization (Fig. 2B and C). Since there was also a decrease in minimum

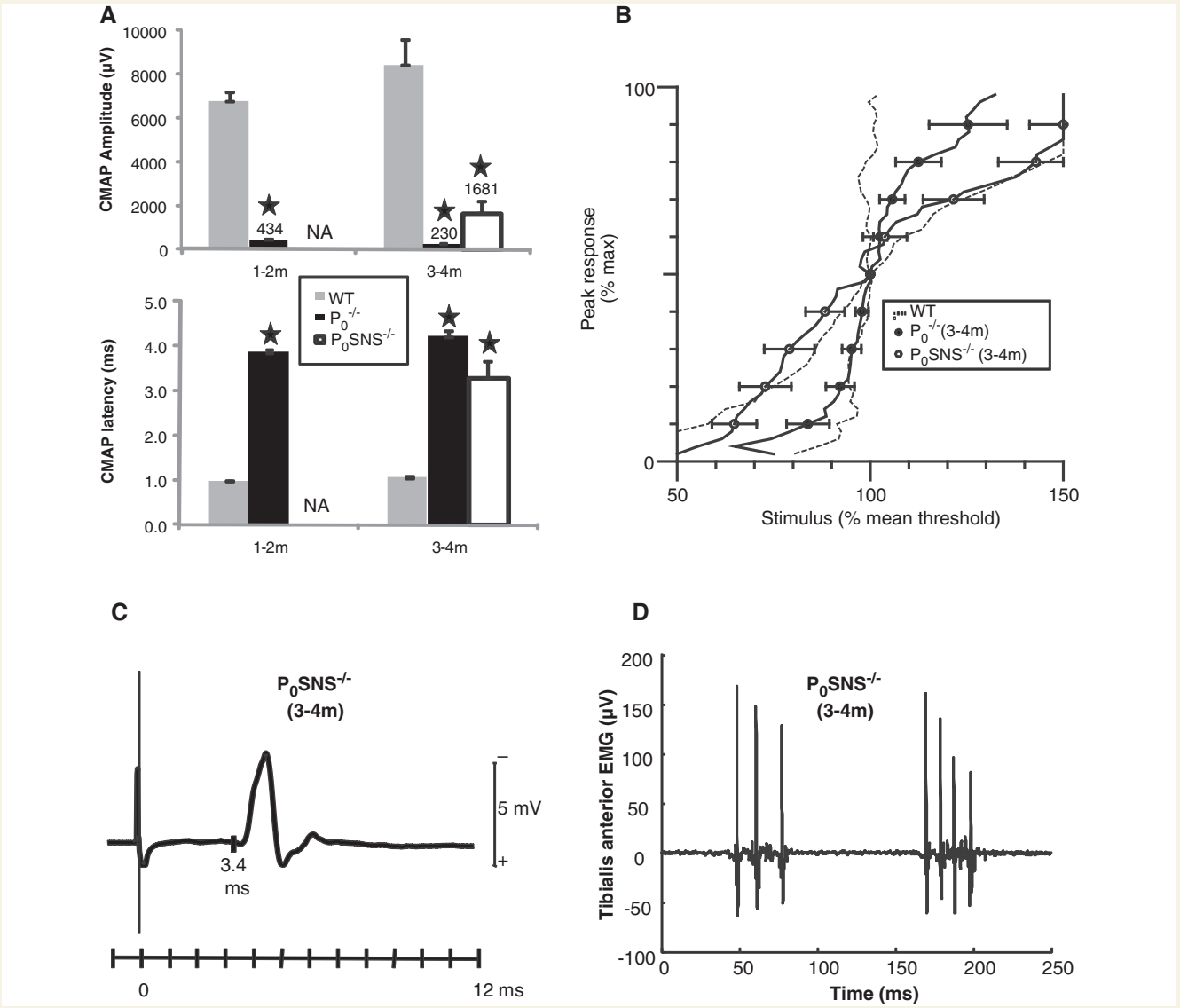

Figure 1 Motor conduction studies of the tibial nerve. (**A**) CMAP amplitudes and latencies for wild-type (WT) and $P_0^{-/-}$ mice were compared at 1–2 months and 3–4 months. $P_0SNS^{-/-}$ mutants were only investigated at 3–4 months. The corresponding normalized stimulus-response slopes are presented in (**B**). The largest CMAP recorded in $P_0SNS^{-/-}$ mice is shown in (**C**). The corresponding EMG recording of the anterior tibial muscle is shown in (**D**). The 95% confidence limits for wild-type are illustrated with stippled lines. Error bars represent SEM. Statistical deviation from wild-type (Mann–Whitney, $P < 0.05$) is indicated with filled stars.

I/V slope by 62% (Fig. 2C, Mann–Whitney $P < 0.01$), it was likely that abnormal passive cable properties made an important contribution to the decreased excitability of $P_0^{-/-}$ nerves.

As compared with wild-type mice, threshold electrotonus (Fig. 2B) and current-threshold relationship in $P_0^{-/-}$ mice (Fig. 2C) showed smaller threshold deviations during depolarization, in contrast with larger deviations during hyperpolarization. The reduction in TEd(90–100 ms) by 17% of threshold (Fig. 2B, Mann–Whitney $P < 0.01$) occurred in parallel with an increase in refractoriness by 43% of threshold (Fig. 2D, Mann–Whitney $P < 0.01$). These excitability measures are very sensitive to membrane potential, and their concordant deviation was shown to occur during membrane depolarization (Kiernan and Bostock, 2000; Moldovan and Krarup, 2004). Hence, apart from alterations in passive membrane properties, $P_0^{-/-}$ motor axons also showed a depolarizing shift in the resting membrane potential.

To further investigate to what extent depolarization contributed to the marked increase in strength–duration time constant in $P_0^{-/-}$ mice, we supplemented the multiple excitability protocol with latent addition studies. We found that P_0 motor axons showed an increase in LAh(0.2 ms) by 9% of threshold as compared with wild-type (Mann–Whitney $P < 0.05$, Fig. 2J) consistent with an increased 'persistent' Na^+ current at resting membrane potential that occurs with depolarization.

At 3–4 months the CMAP appeared further delayed and the reduced amplitude was further decreased as compared with 1–2 months (Mann–Whitney $P < 0.01$, Fig. 1B and D). In contrast, no notable changes occurred in excitability (Fig. 2E–H), except

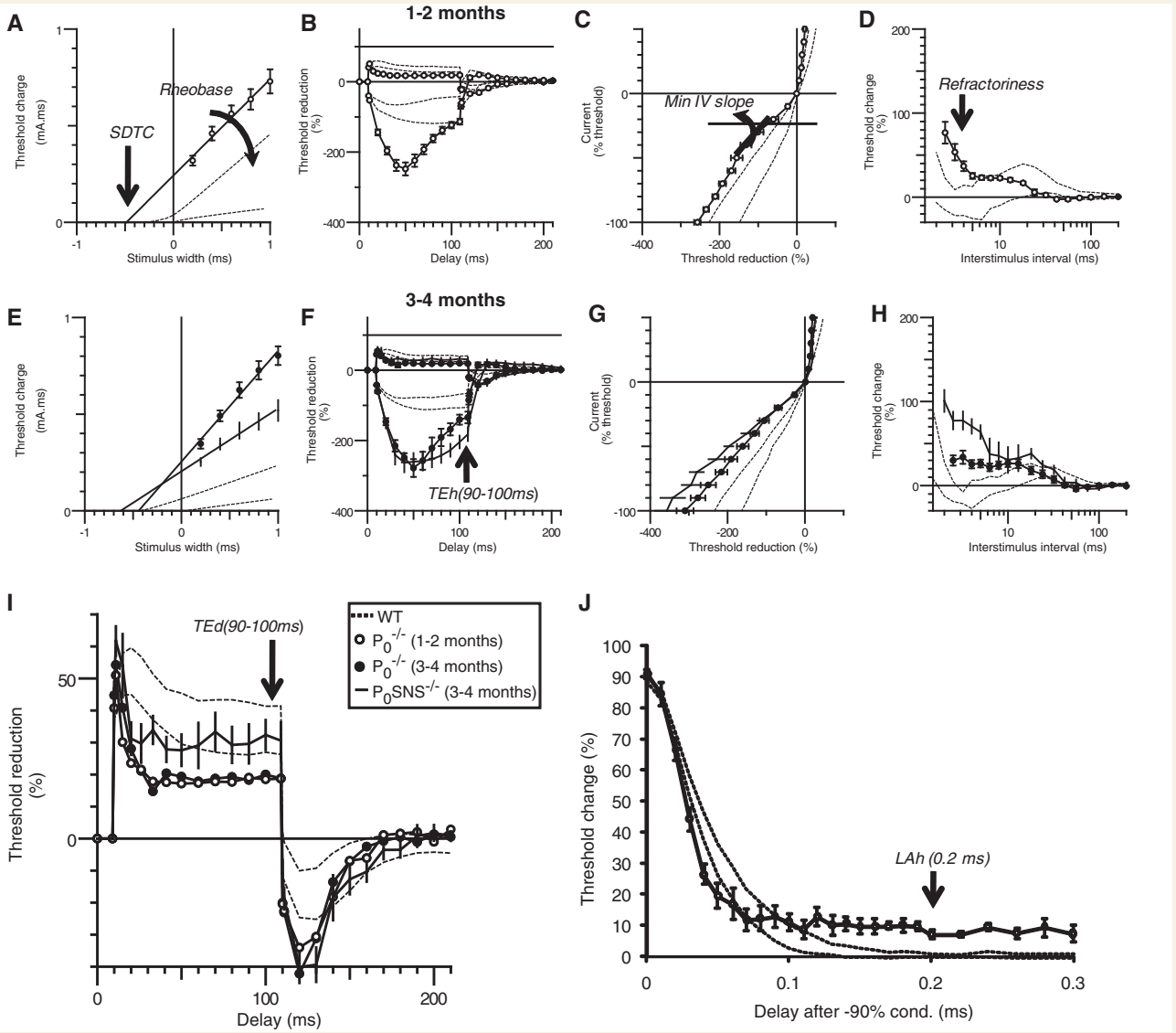

Figure 2 Tibial motor axon excitability in wild-type (WT), $P_0^{-/-}$ and $P_0SNS^{-/-}$ mutants. The complete multiple excitability sequence (charge-duration, threshold electrotonus, current-threshold and recovery cycle) was recorded at 1–2 months (**A–D**) and 3–4 months (**E–H**). The depolarizing threshold electrotonus curves are shown in greater detail in (**I**). The threshold changes during latent-addition are presented in (**J**). Error bars represent SEM. Stippled lines indicate 95% confidence interval of wild-type. SDTC = strength-duration time constant.

for a slight reduction of refractoriness towards wild-type (Mann–Whitney $P < 0.05$, Fig. 2H).

Exploration of excitability abnormalities in myelin protein zero deficient mice

In P_0 deficient mice there was an increased accommodation to depolarization by 8% of threshold and a reduction in accommodation half-time (Fig. 2I, Mann–Whitney $P < 0.05$) suggestive of increased K^+ currents. To explore whether membrane depolarization alone could account for the increase in K^+ currents observed in $P_0^{-/-}$ mice, we carried out additional experiments that are illustrated in Fig. 3.

The direct effect of membrane depolarization on wild-type nerves (age 3–4 months) was studied by applying a depolarizing field using an external stimulator as previously described (Moldovan and Krarup, 2006). At a depolarization level that could reproduce the change in depolarizing electrotonus (Fig. 3A) observed in $P_0^{-/-}$ mice (~20% of threshold) the accommodation to depolarizing electrotonus was slower in depolarized wild-type than in $P_0^{-/-}$ mice (Fig. 3A) suggesting that increased accommodation during depolarization in $P_0^{-/-}$ mice may occur due to an abnormally increased K^+ conductance rather than depolarization. Furthermore, the obtained increase in refractoriness was not associated with a displacement in recovery cycle towards higher thresholds as that seen in $P_0^{-/-}$ mice (Fig. 3C).

It was previously reported in rats, that the effect of K^+ currents on recovery cycle could be enhanced by passing a train of seven conditioning stimuli (RC7) at 4 ms intervals (Schwarz *et al.*, 2006). We applied this protocol to wild-type mice (3–4 months) and

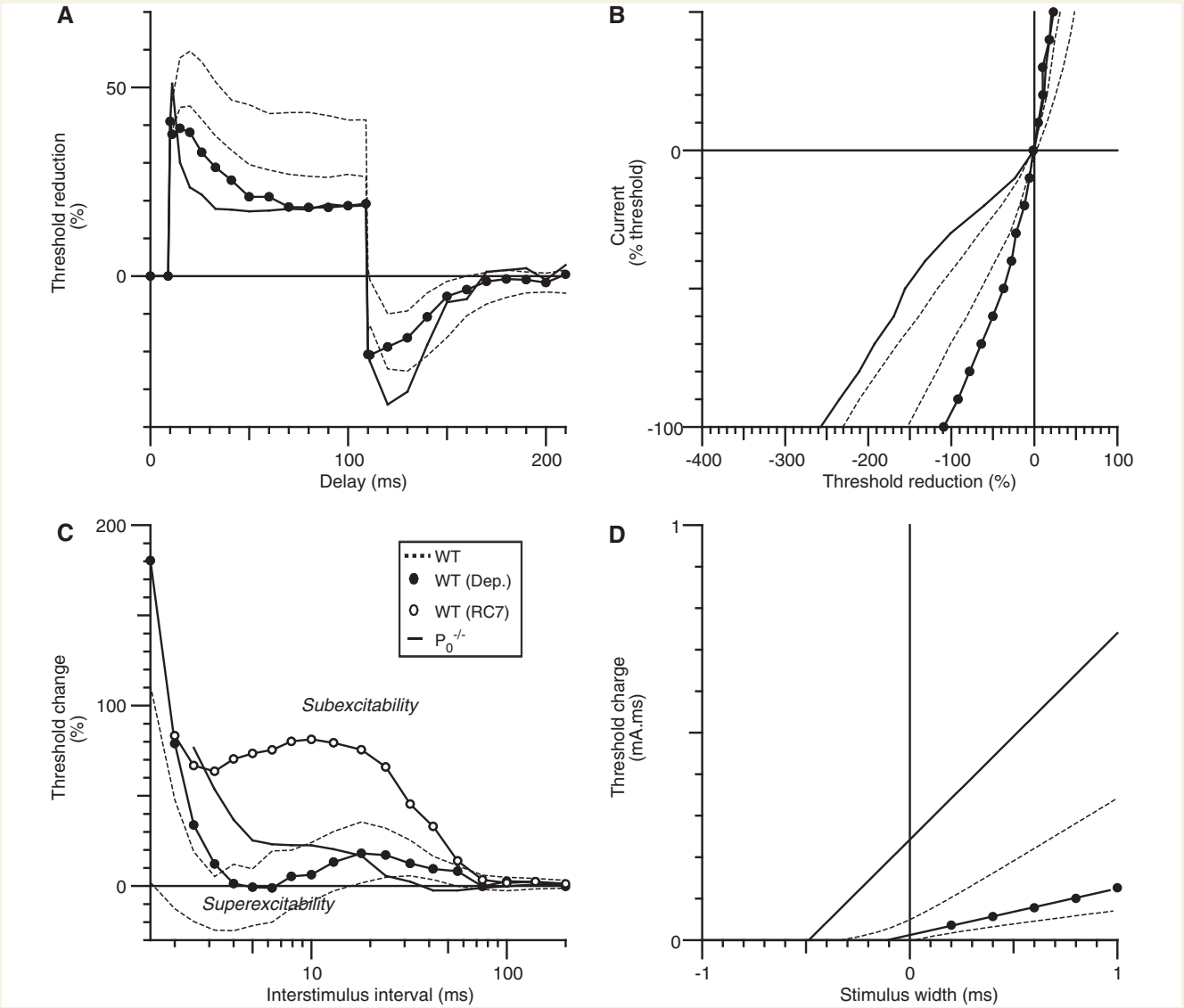

Figure 3 Exploration of the effect of external depolarization (dep; filled symbols) in wild-type (WT) ($n = 4$) as compared with $P_0^{-/-}$ (1–2 months). The complete multiple excitability sequence was recorded: depolarizing threshold electrotonus (**A**), current-threshold (**B**), recovery cycle (**C**) and strength-duration (**D**). Stippled lines indicate 95% confidence interval of wild-type. The changes in recovery cycle induced by a train of seven conditioning pulses repeated at 4 ms in unpolarized wild-type (RC7) are illustrated with open symbols.

found that there was a displacement towards higher thresholds reminiscent of $P_0^{-/-}$ mice (Fig. 3C).

These observations indicated that apart from abnormal passive membrane properties and abnormal Na^+ currents, $P_0^{-/-}$ mice also had increased K^+ currents due to an abnormal K^+ conductance.

Effect of A-803467 on conduction and excitability in myelin protein zero mutants

Although abnormal strength-duration properties were suggestive of abnormal nodal Na^+ currents in $P_0^{-/-}$ mice, these studies alone could not distinguish the contribution of $Na_V1.8$.

The acute effect of A-803467 was investigated in $P_0^{-/-}$ mice at age 3–4 months. No significant changes in either conduction or excitability were observed at 50 mg/kg ($n = 4$, data not shown). Within 2 h following 100 mg/kg A-803467 there was a progressive enlargement of CMAP (Fig. 4A) measured as an increase in peak-to-peak amplitude from 203 ± 58 to $343 \pm 100\,\mu V$ (Wilcoxon, $P < 0.05$). This improvement in amplitude was not associated with a change in latency (Fig. 4A) and was larger in nerves with greater reduction of CMAPs prior to A-803467 (Fig. 4B).

In parallel with an improvement in CMAP, $P_0^{-/-}$ mice showed an improvement in strength-duration properties with a reduction in rheobase by 30% (Fig. 4C, Wilcoxon, $P < 0.05$). The changes in strength–duration time constant and TEd(90–100 ms) were not

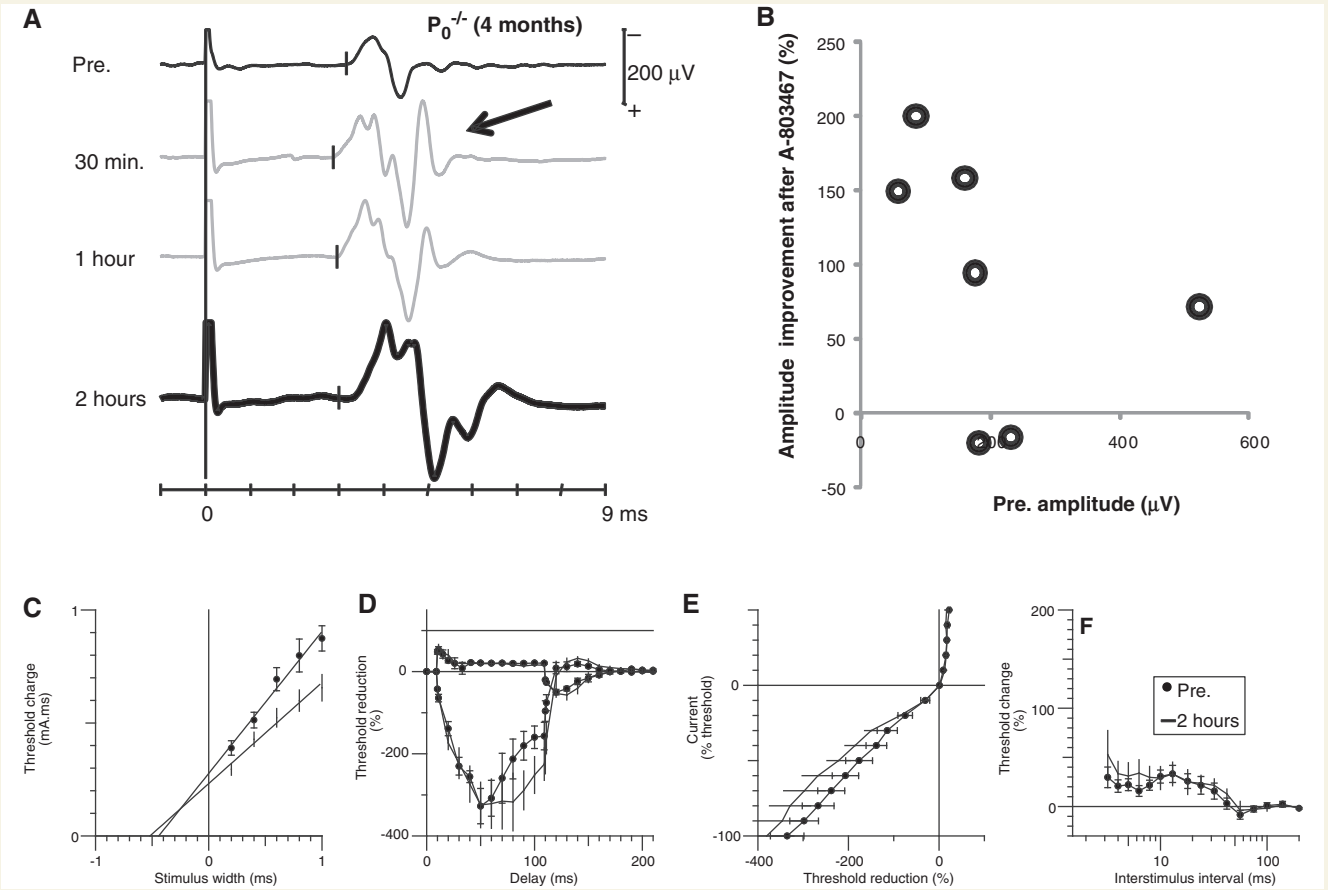

Figure 4 $Na_V1.8$ blocker A-803467 improves conduction and excitability in P_0 deficient mice at four months ($n = 7$). A representative CMAP recording in $P_0^{-/-}$ pre- and up to 2 h post A-803467 (100 mg/kg) is presented in **A**. Note that A-803467 unblocks conduction in some axons (arrow). (**B**) The improvement of CMAP amplitude appeared more pronounced in severely reduced CMAPs. The complete multiple excitability sequence was recorded: strength-duration (**C**), polarizing threshold electrotonus (**D**), current-threshold (**E**) and recovery cycle (**F**). Error bars represent SEM.

significant. Nevertheless, the increase in excitability following A-803467 was paralleled by an apparent alteration of accommodation to hyperpolarization (Fig. 4D) measured as an increase in TEh(90–100 ms) without a change in TEh(20–40 ms). Furthermore, there was an apparent aggravation of the displacement of the early recovery cycle towards higher thresholds (Fig. 4F) reminiscent of the recovery cycle recorded in $P_0^{-/-}$ mice at age 1–2 months (Figs 2D and 3C). Hence, it is likely that the observed changes in excitability reflected, at least in part, the additional contribution to the tracked CMAP of axons unblocked by A-803467.

Similar effects of A-803467 (100 mg/kg) on CMAP and excitability were not observed in wild-type ($n = 4$, data not shown) and $SNS^{-/-}$ mutants ($n = 5$, data not shown).

To investigate whether the improvement in CMAP amplitude could be related to an effect of A-803467 on spontaneous activity we carried out an additional control experiment in three $P_0^{-/-}$ mice (3–4 months old), as illustrated in Fig. 5. Spontaneous activity was recorded from the anterior tibial muscle by a concentric needle. The spontaneous activity consisted of bursts of high frequency discharges (up to 150 Hz) repeated at 4–7 times per second that continued for hours. In all investigated mice, injection of A-803467 (100 mg/kg) had no effect on discharge patterns (Fig. 5A and B) or mean discharge frequency (Fig. 5C), in spite of the prompt increase in CMAP (Fig. 5D).

Effect of $Na_V1.8$ blocker A-803467 on motor performance in myelin protein zero mutants

The rotor-rod endurance time was 287 ± 14 s in wild-type mice at 1–2 months of age ($n = 9$). In contrast, the rotor-rod endurance time was only 64 ± 7 s (Mann–Whitney $P < 0.05$) in $P_0^{-/-}$ mice at 1–2 months ($n = 21$) and it was further reduced to 22 ± 2 s (Mann–Whitney $P < 0.05$) at 3–4 months ($n = 16$). Thus, $P_0^{-/-}$ mice had a motor performance below 10% of wild-type, in good agreement with the magnitude of amplitude impairment of tibial CMAP.

The effect of A-803467 (100 mg/kg) on motor performance was investigated in 4–5 month-old mice (Fig. 6A). The performance of $P_0^{-/-}$ mice was nearly doubled both after 1 h and 2 h

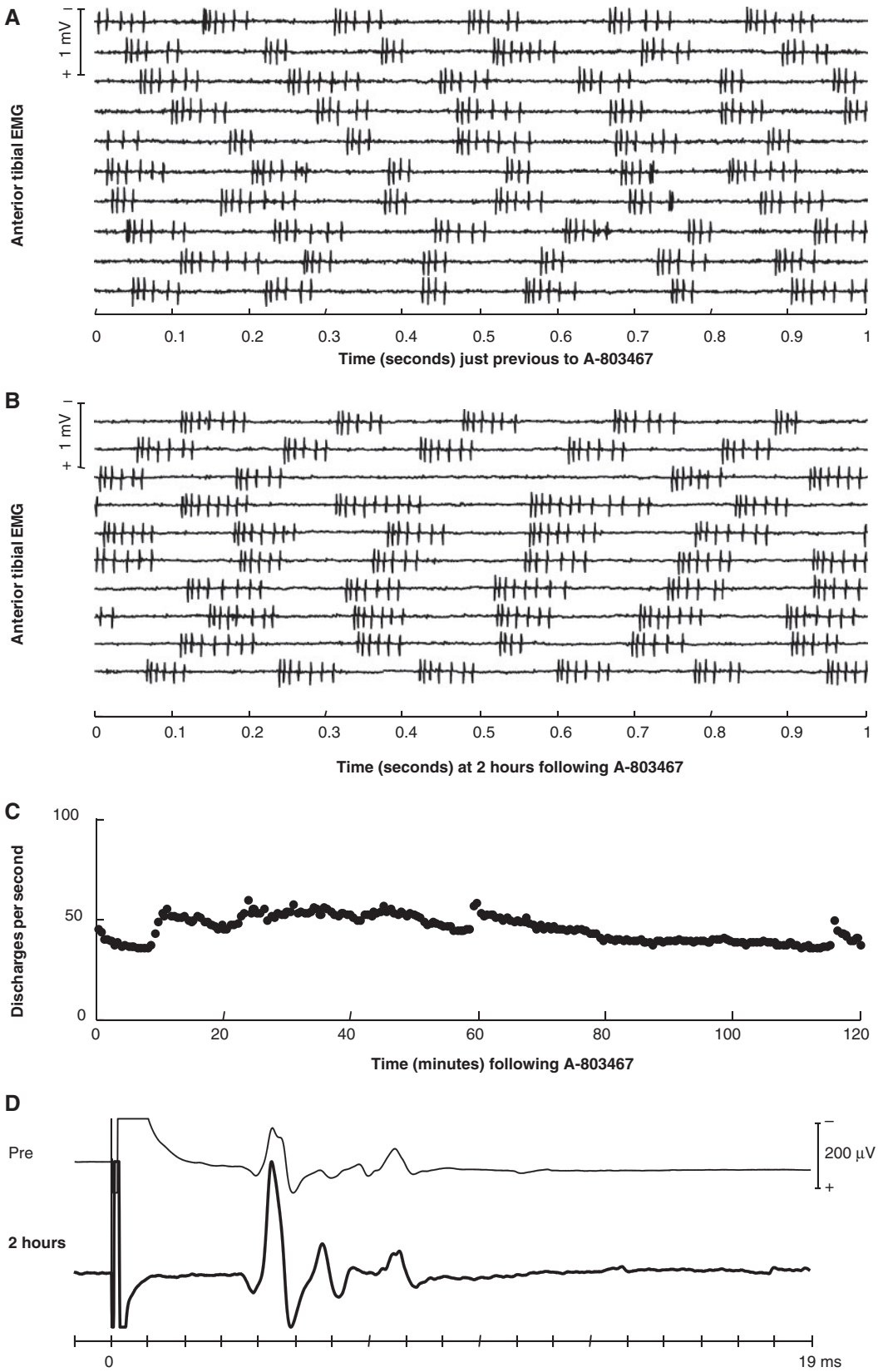

Figure 5 $Na_V1.8$ blocker A-803467 did not alter spontaneous EMG activity in $P_0^{-/-}$. A concentric needle was inserted into the anterior tibial muscle. The discharge pattern was monitored continuously from just before injection of A-803467 (100 mg/kg) for 2 h. A 10 s raster display of discharge patterns from such an experiment are illustrated in (**A**) and (**B**), respectively. The discharge frequency was quantified by thresholding of the rectified signal and averaged in 30 s epochs (**C**). The efficiency of A-803467 administration was monitored by changes in CMAP amplitude (**D**).

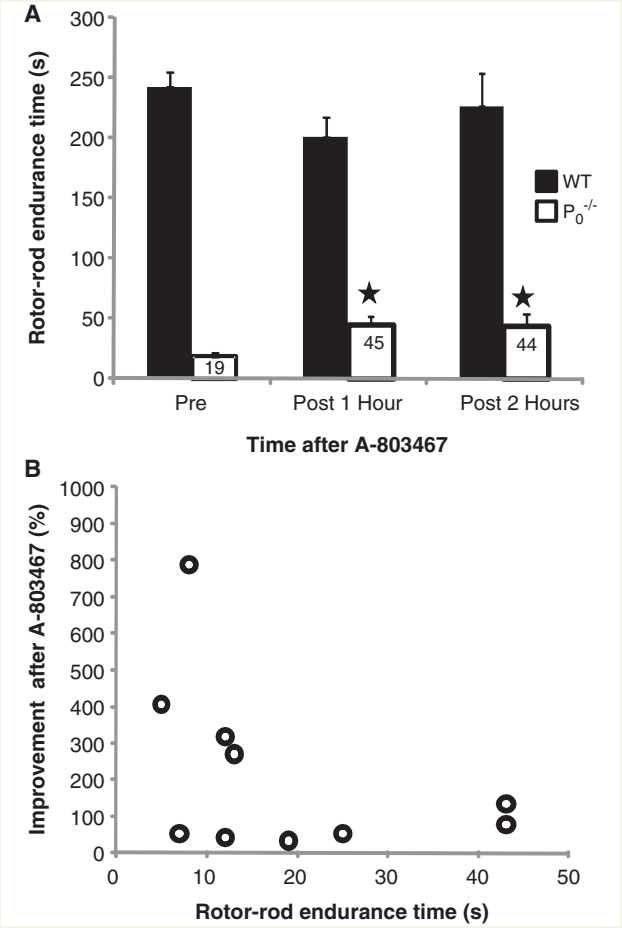

Figure 6 $Na_V1.8$ blocker A-803467 acutely improves motor performance in 4-month-old P_0 deficient mice. In (**A**), the rotor-rod endurance time was compared in $P_0^{-/-}$ mutants ($n = 10$) and wild-type ($n = 12$) at 1 and 2 h following A-803467 (100 mg/kg). In (**B**) the best improvement in rotor-rod endurance time in $P_0^{-/-}$ mice following A-803467 is plotted against the baseline (Pre) rotor-rod endurance time. Error bars represent SEM. Statistical significance (Mann–Whitney, $P < 0.05$) is indicated with stars.

following A-803467 administration (Wilcoxon, $P < 0.05$, Fig. 6B). The improvement was larger in mice with poorer motor performance prior to A-803467 (Fig. 6B), similar to the improvement in tibial nerve CMAP amplitude (Fig. 4B). No effect of A-803467 could be observed in wild-type mice.

Conduction and excitability abnormalities in myelin protein zero, slowly inactivating, tetrodotoxin resistant $Na_V1.8$ voltage gated sodium channel isoform homozygous mutants

Motor conduction and excitability in $SNS^{-/-}$ mutants were undistinguishable from wild-type ($n = 6$, data not shown).

$P_0SNS^{-/-}$ double mutants were only investigated at 3–4 months. The CMAP of $P_0SNS^{-/-}$ mice, although reduced as compared with wild-type, had a 600% higher amplitude (Mann–Whitney $P < 0.01$, Fig. 1A and C) and the latency was ~20% shorter (Mann–Whitney $P < 0.05$, Fig. 1A and C) as compared with $P_0^{-/-}$ mice. To further explore whether these changes in CMAP were associated with an increase in the number of functioning motor units, we compared the normalized stimulus response slopes (Kiernan *et al.*, 2000) and found that the slope was 19 ± 2 in $P_0^{-/-}$ and only 2 ± 1 in $P_0SNS^{-/-}$ mice (Mann–Whitney $P < 0.01$, Fig. 1B), indicating a larger number of functioning motor units in $P_0SNS^{-/-}$ mice.

$P_0SNS^{-/-}$ mice showed spontaneous EMG activity (Fig. 1D) and excitability deviations similar to $P_0^{-/-}$ mice (Fig. 2), most notably the faster accommodation to depolarization measured as a reduction in accommodation half-time as compared with wild-type (Fig. 2E, Mann–Whitney $P < 0.05$), suggestive of similar abnormal K^+ currents in both single and double P_0 mutants. The other excitability measures in $P_0SNS^{-/-}$ mice deviated from wild-type in the same direction as $P_0^{-/-}$ mice, albeit of a smaller magnitude. $P_0SNS^{-/-}$ mice at age 3–4 months had a smaller increase in rheobase (Mann–Whitney $P < 0.05$, Fig. 2E), paralleled by an apparent reduction in accommodation to hyperpolarization (Fig. 2F) and an aggravation of the displacement of early the recovery cycle towards higher thresholds (Fig. 2H) reminiscent of recovery cycle recorded in $P_0^{-/-}$ mice at age 1–2 months (Fig. 2C). These differences were also remarkably similar to those induced in $P_0^{-/-}$ mice by A-803467 (Fig. 4C–F). Nevertheless, in contrast to $P_0^{-/-}$, $P_0SNS^{-/-}$ mice also showed a nearly preserved TEd (90–100 ms) (Fig. 3I), which was not observed within 2 h after A-803467 (Fig. 4D).

Morphological studies

In wild-type mice, the tibial nerve at the ankle contained 1647 ± 30 myelinated axons (Fig. 7A–C). At five months, the mean axonal diameter was 2.5 ± 0.1 μm (Fig. 7B) and the mean myelin thickness was 0.72 ± 0.01 μm (Fig. 7C). The increase in myelin thickness with axonal diameter could reasonably be described by a logarithmic relationship (Fig. 7C).

At five months, tibial nerves of $P_0^{-/-}$ mice contained only 1064 ± 47 axons (Mann–Whitney $P < 0.01$, Fig. 7D–F), although the hallmarks of ongoing degeneration were scarce (Fig. 7D). The mean axonal diameter was decreased to 1.92 ± 0.05 μm (Mann–Whitney $P < 0.01$, Fig. 7E) and the corresponding myelin thickness was decreased to 0.49 ± 0.03 μm (Mann–Whitney $P < 0.01$, Fig. 7E). Apart from the smaller axonal diameter and hypomyelination, some axons showed distinctly abnormal myelin sheaths (either too thick or extremely thin) reflected by the large scatter in the axonal diameter versus myelin thickness relationship (Fig. 7F).

Knocking-out $Na_V1.8$ did not have a major impact on axonal survival of $P_0^{-/-}$ mice within the investigated timeframe. At five months, tibial nerves of $P_0SNS^{-/-}$ mice had a reduced number of myelinated axons to 1024 ± 124 (Mann–Whitney $P < 0.01$, Fig. 7G–I), indistinguishable from $P_0^{-/-}$ mice. Furthermore, in $P_0SNS^{-/-}$ mutants the reduction in axonal

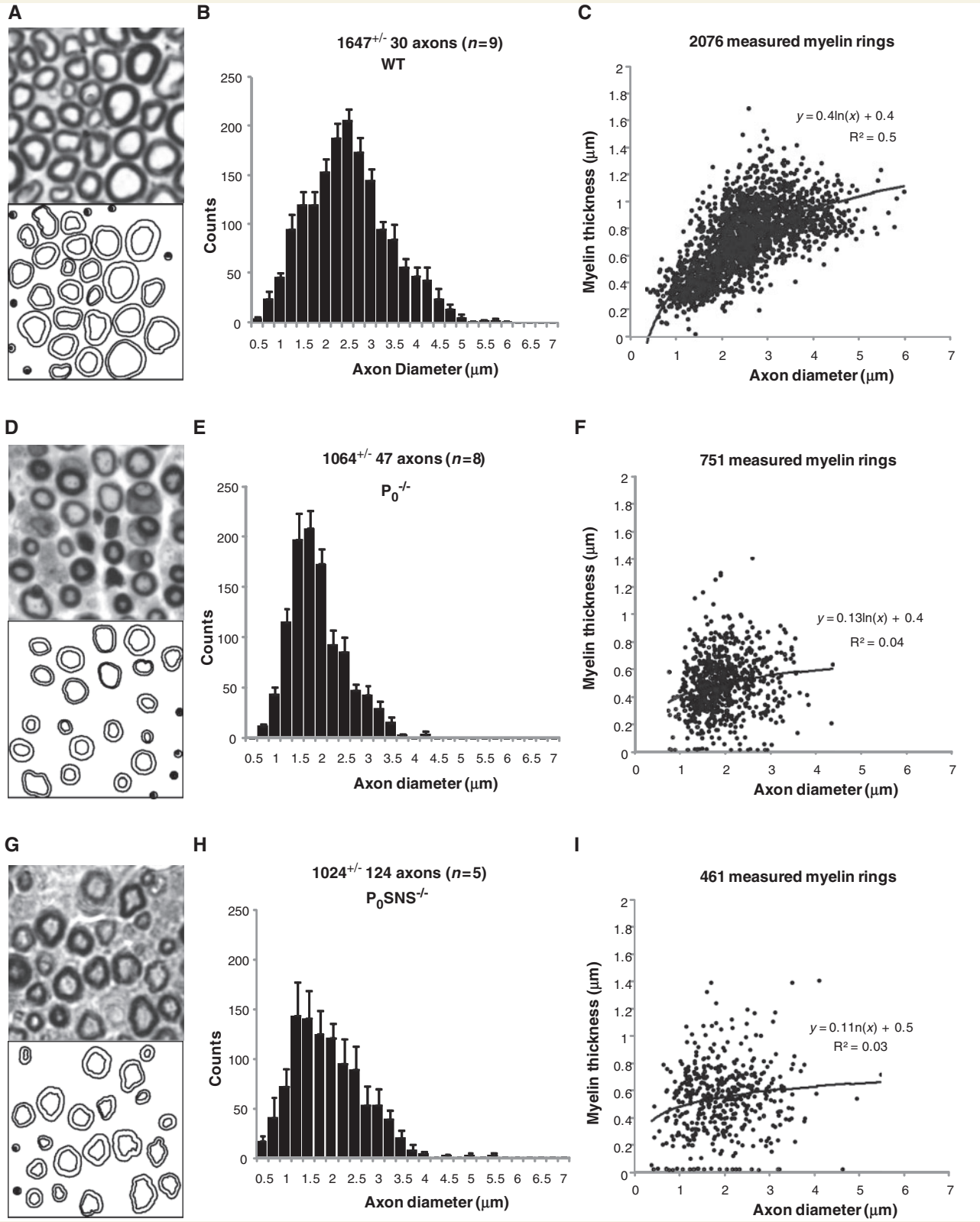

Figure 7 Comparison of myelinated motor axons in wild-type (**A–C**), $P_0^{-/-}$ (**D–F**) and $P_0SNS^{-/-}$ (**G–I**) mice at five months. Panels on the left (**A**, **D** and **G**) show images and the corresponding tracings of myelinated axon-profiles with the corresponding handling of incomplete myelin rings (counted but not included in measurements). Areas shown are 25 μm × 25 μm although only areas >100 μm^2 were actually used for quantification. Middle panels (**B, E** and **H**) present axonal distribution histograms of the total number of axons. The panels on the right (**C**, **F** and **I**) present the relationship between myelin thickness and axonal diameter of the measured axons pooled from all nerves. Error bars represent SEM.

diameter (Fig. 7H) and hypomyelination (Fig. 7I) was similar to that of $P_0^{-/-}$ mice. Although $P_0SNS^{-/-}$ mutants appeared to have slightly more axons $<3\,\mu m$ ($12.5 \pm 2\%$, Fig. 7H) as compared with $P_0^{-/-}$ mutants (8.3 ± 1.9 %, Fig. 7E), this difference was not significant.

In order to further investigate whether $P_0SNS^{-/-}$ double mutants display similar changes in $K_v1.2$ channel distribution as the genuine $P_0^{-/-}$ single mutants (Ulzheimer *et al.*, 2004), we performed double immunofluorescence on teased fibre preparations of quadriceps nerves from wild-type, $P_0^{-/-}$ mutants, and $P_0SNS^{-/-}$ double mutants using antibodies to $K_v1.2$ and Caspr (the latter being a paranodal marker). As expected, in teased fibres of wild-type mice, the vast majority of $K_v1.2$ channels were localized at juxtaparanodal sites (Fig. 8A and E). Corroborating our previous study (Ulzheimer *et al.*, 2004), in $P_0^{-/-}$ mutants, there was a substantial delocalization of the channels comprising the categories of asymmetric distribution or complete absence of signals (Fig. 8B–D). These changes were similar to

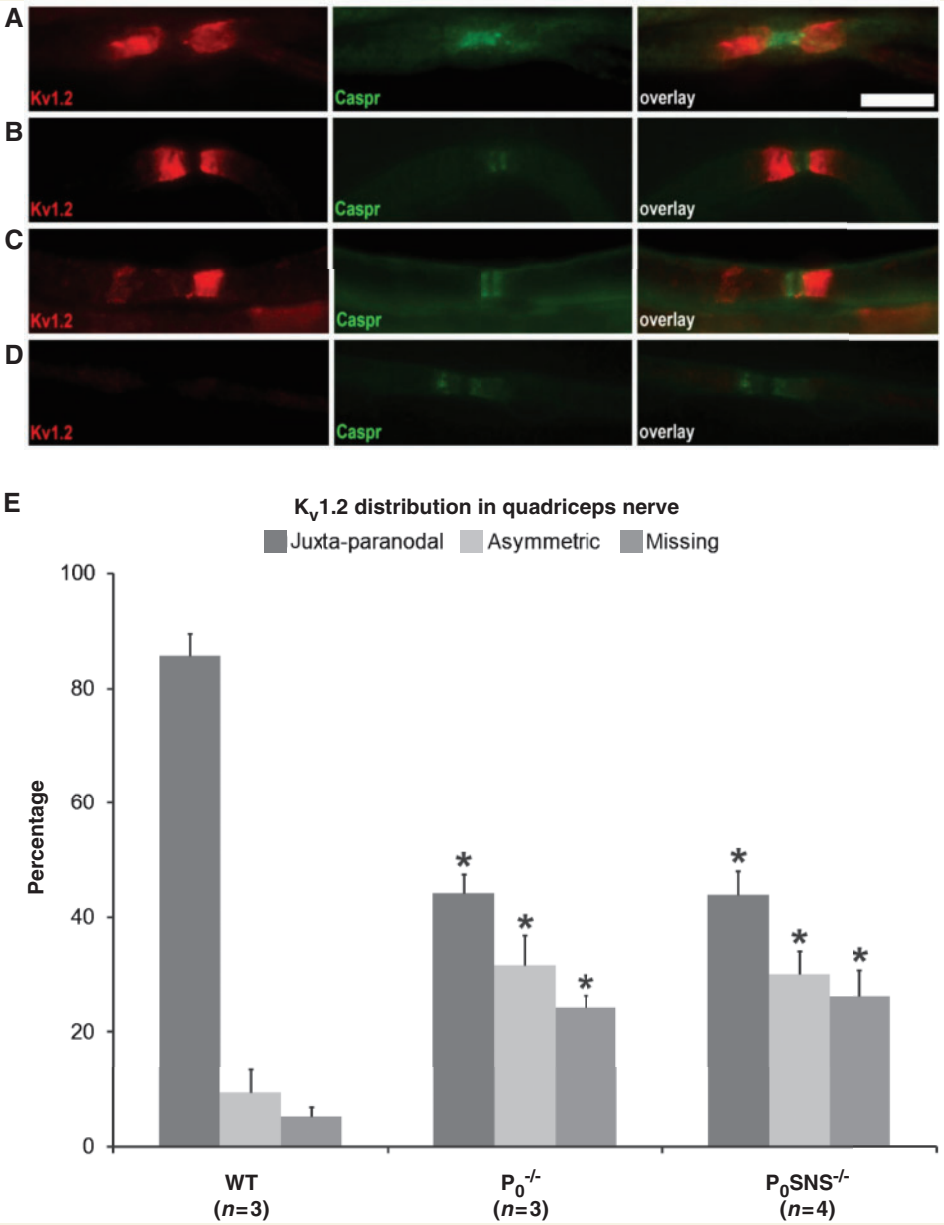

Figure 8 $K_v1.2$ localization in single fibre preparations of quadriceps nerves of wild-type (WT), $P_0^{-/-}$ single mutants and $P_0SNS^{-/-}$ double mutants. Representative staining in wild-type (**A**) and $P_0^{-/-}$ mutants: (**B**) juxta-paranodal distribution, (**C**) asymmetric distribution and (**D**) missing distribution (scale bar = 20 μm). The quantitative distribution is presented in (**E**). Note predominant juxta-paranodal distribution of $K_v1.2$ channels in teased fibres from wild-type mice. In comparison with wild-type mice, there is significantly altered $K_v1.2$ channel distribution in both $P_0^{-/-}$ single mutants and $P_0SNS^{-/-}$ double mutants. The differences between the categories of either mutant are not significant ($P > 0.5$, Student's *t*-test). $^*P < 0.01$ in comparison to wild-type mice. *n* = number of mice investigated.

those quantified in the $P_0SNS^{-/-}$ double mutants, as reflected by non-significant differences between the categories of either mutant (Fig. 8E). Hence these data demonstrate that $K_v1.2$ channel distribution is similar in $P_0^{-/-}$ mutants in comparison to $P_0SNS^{-/-}$ double mutants and can, therefore, not explain the physiological differences seen in the single versus double mutants.

Discussion

We assessed the functional impairment of P_0-deficient motor axons with particular emphasis on $Na_v1.8$ voltage gated sodium channel function. We found that in the context of dysmyelination abnormal K^+ currents and membrane depolarization, the ectopic $Na_V1.8$ channels further impaired the motor axon excitability in $P_0^{-/-}$ mice to an extent that precipitated conduction failure in severely affected axons.

An altered expression of neuronal voltage gated sodium channels was previously reported following axonal injury both in peripheral (Dib-Hajj *et al.*, 1996; Cummins and Waxman, 1997; Sleeper *et al.*, 2000) and central (Hains and Waxman, 2007) sensory neurons. During normal development the onset of myelination triggers a change from the immature to mature voltage gated sodium channels isoform repertoire (Waxman *et al.*, 1994; Boiko *et al.*, 2001) dependent on myelin-axon interactions (Bremer *et al.*, 2010). This process seems to be reversed, at least in part, during demyelinating disorders (Black *et al.*, 1999, 2000). It was therefore suggested that the 'transcriptional voltage gated sodium channels channelopathies' that occur in various pathological conditions may primarily reflect dynamic changes in axon-glial interactions during the processes of demyelination and remyelination (Waxman, 2000, 2001).

An increasing body of evidence suggests that voltage gated sodium channel channelopathies in sensory neurons may be associated with abnormal excitability and pain (Dib-Hajj *et al.*, 2009). Our findings raise the novel possibility that a voltage gated sodium channels channelopathy occurring in the context of dysmyelination may also impair the function of motor axons. We propose that $Na_V1.8$ channels may be a novel therapeutic target in human hereditary neuropathies.

$Na_V1.8$ contributes to impaired motor axon excitability in myelin protein zero deficient mice

The most consistent excitability abnormality in $P_0^{-/-}$ mice was an overall reduction in excitability measured by an increased rheobase, as compared with age-matched wild-type. It was previously reported that nerves of $P_0^{-/-}$ mice have reduced excitability, as reflected by a very high threshold for action potential generation (Zielasek *et al.*, 1996). Nevertheless, while threshold is a global measure of nerve excitability (Bostock *et al.*, 1998), strength-duration properties are primarily dependent on the function of the nodal voltage gated sodium channel (Mogyoros *et al.*, 1996, 2000).

$Na_V1.8$ knock-out caused an improvement in excitability measured as a reduction in rheobase in $P_0^{-/-}$ mice. It is unlikely that this effect could be attributed to indirect compensatory changes in double mutants—e.g. by other changes in voltage gated sodium channel isoforms (Akopian *et al.*, 1999)—since pharmacological block of $Na_V1.8$ with A-803467 (Jarvis *et al.*, 2007) led to an acute improvement of both tibial nerve excitability and motor function of $P_0^{-/-}$ mutants. Hence, our electrophysiological studies in $P_0^{-/-}$, $P_0SNS^{-/-}$ and $P_0^{-/-}$ mice treated with the respective pharmacological inhibitors, strongly support previous observations in $P_0^{-/-}$ mice of $Na_V1.8$ expression in motor axons (Ulzheimer *et al.*, 2004). Furthermore, here we present novel evidence that this ectopic $Na_V1.8$ expression is also detrimental for motor axons. Of note, we could recently recapitulate the ectopic $Na_v1.8$ expression in ventral aspects of spinal cords from $P_0^{-/-}$ mice by polymerase chain reaction using $Na_v1.8$-specific primers (Klein D. and Martini R., unpublished observations).

An increased $Na_V1.8$ expression was also found in another dysmyelinating mutant, the Trembler-J (Devaux and Scherer, 2005). However, in contrast to our study, $Na_V1.8$ could not be localized on motor axons in ventral roots. More studies may be necessary in Trembler-J mutant mice, possibly investigating motor nerves rather than roots, using more direct electrophysiological approaches and investigating Trembler-J/SNS double mutant mice.

It is important to note that under injury conditions, $Na_V1.8$ is downregulated, which could be viewed as being in conflict with our study (Decosterd *et al.*, 2002). However, based on the recent observation that $Na_V1.8$ can be locally upregulated in injured axons (Thakor *et al.*, 2009), it is possible that P_0 mutant Schwann cells can locally influence membrane localization of $Na_V1.8$ on axons. Future studies focusing on the corresponding mechanisms might be of major interest.

$Na_V1.8$ precipitates conduction failure in myelin protein zero deficient mice

Previous nerve conduction studies in $P_0^{-/-}$ mice revealed markedly delayed CMAPs of reduced amplitude and increased duration (Zielasek *et al.*, 1996) consistent with hypomyelination and axonal loss (Lewis *et al.*, 2000).

Here we found that in $P_0^{-/-}$ mice, reduced motor performance at rotor-rod below 10% of wild-type (Fig. 4) was associated with a reduction in tibial nerve CMAP below 10% (Fig. 1), in marked contrast with only 40% reduction in number of myelinated axons (Fig. 7). Previous studies have suggested that this discrepancy could be explained by distal changes of motor branches (Frei *et al.*, 1999; Ey *et al.*, 2007) that retract and regenerate dysfunctional synaptic terminals, as seen in dysmyelinating transgenic mice that overexpress P_0 (Yin *et al.*, 2004).

Since, with acute pharmacological $Na_V1.8$ block, there is an increase in CMAP amplitude (Fig. 4A and B) and an improvement in motor performance at rotor-rod (Fig. 6A), our data suggest that in an important fraction of the dysmyelinated motor axons, the conduction failure is functional, and thus potentially reversible.

We cannot exclude that part of the improvement induced by A-803467 on rotor-rod performance was related to an additional effect on sensory axons that were also found to be abnormal in $P_0^{-/-}$ mice (Samsam *et al.*, 2002, 2003; Ulzheimer *et al.*, 2004).

Nevertheless, the A-803467 effect on motor axons is strongly indicated by the increase in CMAP amplitude and motor excitability changes (Fig. 4) that occurred independent of changes in spontaneous activity (Fig. 5). Furthermore, as compared with $P_0^{-/-}$, $P_0SNS^{-/-}$ mice have larger CMAP amplitudes (Fig. 1A and C) associated with an increase in number of functioning motor units (Fig. 1B). Thus, it is likely that the ectopic presence of $Na_V1.8$ impairs excitability and precipitates conduction failure in severely affected $P_0^{-/-}$ motor axons.

On the mechanism of conduction failure in myelin protein zero deficient mice

Excitability measures in $P_0^{-/-}$ mice, most notably TEd(90–100 ms) (Kiernan and Bostock, 2000; Moldovan and Krarup, 2004) were suggestive of a depolarizing shift in membrane potential. We find it reasonable to suspect that in the context of depolarization, abnormal K^+ currents may 'clamp' the action potential and lead to depolarizing conduction block (Kaji, 2003; Priori *et al.*, 2005). Nevertheless, both $P_0^{-/-}$ and $P_0SNS^{-/-}$ mice showed functional evidence of abnormal K^+ currents: a faster accommodation to depolarization and displacement towards higher thresholds of the early recovery cycle following an action potential. Furthermore, we found that the profound disorganization of paranodal $K_v1.2$ channels in $P_0^{-/-}$ single mutants (Ulzheimer *et al.*, 2004) was similar in $P_0SNS^{-/-}$ double mutants (Fig. 8). Taken together, these observations suggest that abnormal K^+ currents could not account for the functional differences between $P_0^{-/-}$ and $P_0SNS^{-/-}$ mice.

It remains plausible that in the context of depolarization, increased Na^+ influx via slow inactivating $Na_V1.8$ voltage gated sodium channels would further aggravate depolarization and precipitate conduction failure in $P_0^{-/-}$ and not in $P_0SNS^{-/-}$ mice, where the larger CMAP amplitude was indeed associated with a near-normal TEd(90–100 ms). Nevertheless, it should be noted that in spite of similar number and morphology of axons in $P_0^{-/-}$ mice compared with $P_0SNS^{-/-}$, this improvement in TEd (90–100 ms) was not significant after acute pharmacologic $Na_V1.8$ block. A smaller threshold decrease in depolarization was previously reported in intoxication with tetrodotoxin, in agreement with a mathematical model of myelinated motor axons (Kiernan *et al.*, 2005). Nevertheless, $Na_V1.8$ seems to be coexpressed with $Na_V1.6$ on $P_0^{-/-}$ motor axons (Ulzheimer *et al.*, 2004) and an upregulation rather than a downregulation of tetrodotoxin-sensitive Na^+ channels was reported in sensory axons in $Na_V1.8$ knock-outs (Akopian *et al.*, 1999). Thus, considering also the smaller improvement of amplitude in $P_0^{-/-}$ mice as compared with $P_0SNS^{-/-}$, it remains possible that the dose of 100 mg/kg A-803467 was submaximal. However, we did not increase the dose further due to selectivity concerns (Jarvis *et al.*, 2007).

Hence, these observation suggest that $Na_V1.8$ ectopic expression is able to precipitate conduction failure specifically in connection with the other severe membrane abnormalities that are present in $P_0^{-/-}$.

The role of ion channel dysfunction in progression of neuropathy in myelin protein zero deficient mice

Although prolonged membrane depolarization was found to be detrimental for motor axons (Kiernan *et al.*, 2002) and increased Na^+ influx through voltage gated sodium channels contributes to Na^+ mediated axonal degeneration in immune-mediated demyelination (Bechtold and Smith, 2005), knocking-out $Na_V1.8$ did not seem to have a major impact on the progression of axonal loss in $P_0^{-/-}$ axons, at least in the investigated time-frame. Progression of dysmyelination was also indistinguishable in $P_0^{-/-}$ and $P_0SNS^{-/-}$ mice, consistent with similar excitability deviations attributable to alterations in passive cable, related to demyelination/remyelination (Cappelen-Smith *et al.*, 2001; Nodera *et al.*, 2004; Sung *et al.*, 2004) and shortening of internodes (Moldovan and Krarup, 2004, 2007; Nakata *et al.*, 2008). Furthermore, the acute pharmacological $Na_V1.8$ block and knock-out did not influence the profuse neuromyotonia-like spontaneous EMG activity recorded in P_0-mutants, which is not surprising since a similar spontaneous EMG activity in connection with alterations in K^+ rather than Na^+ channels was reported in the Trembler-J dysmyelinating mutant (Devaux and Scherer, 2005). Taken together, these observations suggest that ectopic $Na_V1.8$ expression is not the primary cause for progression of neuropathy in $P_0^{-/-}$ mice.

In spite of improved excitability and CMAP amplitude, A-803467 induced an apparent increase in the abnormal displacement of recovery cycle in $P_0^{-/-}$ mice, in parallel with reduced accommodation to hyperpolarization (Fig. 4D and F). These changes were remarkably similar to those observed in $P_0SNS^{-/-}$ mice (Fig. 2F and H) and could not be attributed to a procedure related to systemic pharmacological manipulations. Inward rectification was found to be dependent on the investigated axon population (Mori *et al.*, 2010; Tomlinson *et al.*, 2010). Therefore it is more likely that the severely affected $P_0^{-/-}$ axons resume conduction following $Na_V1.8$ antagonism or knock-out and this leads to an apparent aggravation of excitability alterations of the investigated axon population. This is further supported by the observation that the effect of A-803467 on both CMAP (Fig. 4B) and motor performance (Fig. 6B) was greatest in the most affected animals. Thus, it is likely that as the $P_0^{-/-}$ neuropathy progresses, the detrimental effect of $Na_V1.8$ on motor axon function is also greater. Further studies using prolonged treatment with $Na_V1.8$ blockers might clarify this possibility.

Clinical relevance

Upregulation of $Na_V1.8$ channels has also been reported in a nerve biopsy from a severely affected patient with Charcot–Marie–Tooth Type 1B disease, with an R98C (also known as R69C with a different numbering system) (Bai *et al.*, 2006). Thus, both the severe loss of function phenotype and the toxic gain of function phenotype in this heterozygous patient upregulate Nav1.8 channels suggesting that these distinct paths converge at least for this molecule.

$P_0^{-/-}$ mutant mice completely deficient of P_0 have a phenotype resembling that of severely affected patients with Charcot–Marie–Tooth disease (Martini *et al.*, 1995; Martini, 1999). Previous therapeutic approaches in distinct animal models for Charcot–Marie–Tooth disease were aimed at neuroprotection. It is worthwhile to mention in this context that Tacrolimus (FK506), an agent with neuroprotective properties, aggravated axonopathic features in patients (Weimer and Podwall, 2006) and P_0 mutant mice (Ip *et al.*, 2009), thus precluding this option. By contrast, administration of the progesterone receptor antagonist onapristone reduced overexpression of PMP22 and ameliorated neuropathy in a rat model of Charcot–Marie–Tooth Type 1A disease (Sereda *et al.*, 2003; Meyer zu Horste *et al.*, 2007). More recently, Martini and colleagues (2008) suggested that inflammatory cells, particularly macrophages and the pathways leading to their activation might be another promising approach to treat Charcot–Marie–Tooth disorders (Martini *et al.*, 2008).

In the present study, we propose that in particularly severe forms of inherited neuropathies with a dysmyelinating phenotype, improving conduction might be an important alternative therapeutic strategy to neuroprotection. Specifically we propose that acute $Na_V1.8$ blockers may be a novel tool to alleviate symptoms like weakness and poor motor performance in Charcot–Marie–Tooth disease. Further studies should be carried out to investigate to what extent chronic treatment with $Na_V1.8$ blockers may alter the time-course of motor symptoms in Charcot–Marie–Tooth disease.

Acknowledgements

We would like to thank Dr Antje Kroner for genetic advice, Dr Irina Korshunova for help with genotyping the mice and Mrs Lis Hansen for expert technical assistance with histological preparations. We are grateful to Mrs Silke Loserth for excellent technical support and Dr S. Rock Levinson (Denver, Colorado) for helpful discussion.

Funding

Lundbeck Foundation; the Novo Nordisk Foundation; the Danish Medical Research Council; Ludvig and Sara Elsass Foundation; Foundation for Research in Neurology; Jytte and Kaj Dahlbom's Foundation; Interdisciplinary Center for Clinical Research, University of Würzburg.

References

Akopian AN, Sivilotti L, Wood JN. A tetrodotoxin-resistant voltage-gated sodium channel expressed by sensory neurons. Nature 1996; 379: 257–262.

Akopian AN, Souslova V, England S, Okuse K, Ogata N, Ure J, et al. The tetrodotoxin-resistant sodium channel SNS has a specialized function in pain pathways. Nat Neurosci 1999; 2: 541–548.

Bai Y, Ianokova E, Pu Q, Ghandour K, Levinson R, Martin JJ, et al. Effect of an R69C mutation in the myelin protein zero gene on myelination and ion channel subtypes. Arch Neurol 2006; 63: 1787–1794.

Bechtold DA, Smith KJ. Sodium-mediated axonal degeneration in inflammatory demyelinating disease. J Neurol Sci 2005; 233: 27–35.

Black JA, Dib-Hajj S, Baker D, Newcombe J, Cuzner ML, Waxman SG. Sensory neuron-specific sodium channel SNS is abnormally expressed in the brains of mice with experimental allergic encephalomyelitis and humans with multiple sclerosis. Proc Natl Acad Sci USA 2000; 97: 11598–11602.

Black JA, Fjell J, Dib-Hajj S, Duncan ID, O'Connor LT, Fried K, et al. Abnormal expression of SNS/PN3 sodium channel in cerebellar Purkinje cells following loss of myelin in the taiep rat. Neuroreport 1999; 10: 913–918.

Boerio D, Greensmith L, Bostock H. Excitability properties of motor axons in the maturing mouse. J Peripher Nerv Syst 2009; 14: 45–53.

Boerio D, Kalmar B, Greensmith L, Bostock H. Excitability properties of mouse motor axons in the mutant SOD1(G93A) model of amyotrophic lateral sclerosis. Muscle Nerve 2010; 41: 774–784.

Boiko T, Rasband MN, Levinson SR, Caldwell JH, Mandel G, Trimmer JS, et al. Compact myelin dictates the differential targeting of two sodium channel isoforms in the same axon. Neuron 2001; 30: 91–104.

Bostock H. The strength-duration relationship for excitation of myelinated nerve: computed dependence on membrane parameters. J Physiol 1983; 341: 59–74.

Bostock H, Cikurel K, Burke D. Threshold tracking techniques in the study of human peripheral nerve. Muscle Nerve 1998; 21: 137–158.

Bostock H, Rothwell JC. Latent addition in motor and sensory fibres of human peripheral nerve. J Physiol 1997; 498: 277–294.

Bremer J, Baumann F, Tiberi C, Wessig C, Fischer H, Schwarz P, et al. Axonal prion protein is required for peripheral myelin maintenance. Nat Neurosci 2010; 13: 310–318.

Cappelen-Smith C, Kuwabara S, Lin CS, Mogyoros I, Burke D. Membrane properties in chronic inflammatory demyelinating polyneuropathy. Brain 2001; 124: 2439–2447.

Cummins TR, Waxman SG. Downregulation of tetrodotoxin-resistant sodium currents and upregulation of a rapidly repriming tetrodotoxin-sensitive sodium current in small spinal sensory neurons after nerve injury. J Neurosci 1997; 17: 3503–3514.

Decosterd I, Ji RR, Abdi S, Tate S, Woolf CJ. The pattern of expression of the voltage-gated sodium channels Na(v)1.8 and Na(v)1.9 does not change in uninjured primary sensory neurons in experimental neuropathic pain models. Pain 2002; 96: 269–277.

Devaux JJ, Scherer SS. Altered ion channels in an animal model of Charcot-Marie-Tooth disease type IA. J Neurosci 2005; 25: 1470–1480.

Dib-Hajj S, Black JA, Felts P, Waxman SG. Down-regulation of transcripts for Na channel alpha-SNS in spinal sensory neurons following axotomy. Proc Natl Acad Sci USA 1996; 93: 14950–14954.

Dib-Hajj SD, Black JA, Waxman SG. Voltage-gated sodium channels: therapeutic targets for pain. Pain Med 2009; 10: 1260–1269.

Ey B, Kobsar I, Blazyca H, Kroner A, Martini R. Visualization of degenerating axons in a dysmyelinating mouse mutant with axonal loss. Mol Cell Neurosci 2007; 35: 153–160.

Filbin MT, Walsh FS, Trapp BD, Pizzey JA, Tennekoon GI. Role of myelin P0 protein as a homophilic adhesion molecule. Nature 1990; 344: 871–872.

Frei R, Motzing S, Kinkelin I, Schachner M, Koltzenburg M, Martini R. Loss of distal axons and sensory Merkel cells and features indicative of muscle denervation in hindlimbs of P0-deficient mice. J Neurosci 1999; 19: 6058–6067.

Giese KP, Martini R, Lemke G, Soriano P, Schachner M. Mouse P0 gene disruption leads to hypomyelination, abnormal expression of recognition molecules, and degeneration of myelin and axons. Cell 1992; 71: 565–576.

Goldin AL, Barchi RL, Caldwell JH, Hofmann F, Howe JR, Hunter JC, et al. Nomenclature of voltage-gated sodium channels. Neuron 2000; 28: 365–368.

Hains BC, Waxman SG. Sodium channel expression and the molecular pathophysiology of pain after SCI. Prog Brain Res 2007; 161: 195–203.

Herold KF, Nau C, Ouyang W, Hemmings HC Jr. Isoflurane inhibits the tetrodotoxin-resistant voltage-gated sodium channel Nav1.8. Anesthesiology 2009; 111: 591–599.

Hockly E, Woodman B, Mahal A, Lewis CM, Bates G. Standardization and statistical approaches to therapeutic trials in the R6/2 mouse. Brain Res Bull 2003; 61: 469–479.

Ip CW, Kroner A, Kohl B, Wessig C, Martini R. Tacrolimus (FK506) causes disease aggravation in models for inherited peripheral myelinopathies. Neurobiol Dis 2009; 33: 207–212.

Jarvis MF, Honore P, Shieh CC, Chapman M, Joshi S, Zhang XF, et al. A-803467, a potent and selective Nav1.8 sodium channel blocker, attenuates neuropathic and inflammatory pain in the rat. Proc Natl Acad Sci USA 2007; 104: 8520–8525.

Kaji R. Physiology of conduction block in multifocal motor neuropathy and other demyelinating neuropathies. Muscle Nerve 2003; 27: 285–296.

Kiernan MC, Bostock H. Effects of membrane polarization and ischaemia on the excitability properties of human motor axons. Brain 2000; 123: 2542–2551.

Kiernan MC, Burke D, Andersen KV, Bostock H. Multiple measures of axonal excitability: a new approach in clinical testing. Muscle Nerve 2000; 23: 399–409.

Kiernan MC, Isbister GK, Lin CS, Burke D, Bostock H. Acute tetrodotoxin-induced neurotoxicity after ingestion of puffer fish. Ann Neurol 2005; 57: 339–348.

Kiernan MC, Walters RJ, Andersen KV, Taube D, Murray NM, Bostock H. Nerve excitability changes in chronic renal failure indicate membrane depolarization due to hyperkalaemia. Brain 2002; 125: 1366–1378.

Kozak CA, Sangameswaran L. Genetic mapping of the peripheral sodium channel genes, Scn9a and Scn10a, in the mouse. Mamm Genome 1996; 7: 787–788.

Kramer K, Van Acker SA, Grimbergen JA, van den Berg DJ, Van der Vijgh WJ, Bast A. Effect of dimethyl sulfoxide (DMSO) on the electrocardiogram (ECG) in freely moving male Balb/c mice. Gen Pharmacol 1995; 26: 1403–1407.

Krzemien DM, Schaller KL, Levinson SR, Caldwell JH. Immunolocalization of sodium channel isoform NaCh6 in the nervous system. J Comp Neurol 2000; 420: 70–83.

Lewis RA, Sumner AJ, Shy ME. Electrophysiological features of inherited demyelinating neuropathies: a reappraisal in the era of molecular diagnosis. Muscle Nerve 2000; 23: 1472–1487.

Lemke G. The molecular genetics of myelination: an update. Glia 1993; 7: 263–271.

Li J, Bai Y, Ianakova E, Grandis M, Uchwat F, Trostinskaia A, et al. Major myelin protein gene (P0) mutation causes a novel form of axonal degeneration. J Comp Neurol 2006; 498: 252–265.

Marrosu MG, Vaccargiu S, Marrosu G, Vannelli A, Cianchetti C, Muntoni F. Charcot-Marie-Tooth disease type 2 associated with mutation of the myelin protein zero gene. Neurology 1998; 50: 1397–1401.

Martini R. P0-deficient knockout mice as tools to understand pathomechanisms in Charcot-Marie-Tooth 1B and P0-related Dejerine-Sottas syndrome. Ann NY Acad Sci 1999; 883: 273–280.

Martini R, Fischer S, Lopez-Vales R, David S. Interactions between Schwann cells and macrophages in injury and inherited demyelinating disease. Glia 2008; 56: 1566–1577.

Martini R, Schachner M. Molecular bases of myelin formation as revealed by investigations on mice deficient in glial cell surface molecules. Glia 1997; 19: 298–310.

Martini R, Zielasek J, Toyka KV, Giese KP, Schachner M. Protein zero (P0)-deficient mice show myelin degeneration in peripheral nerves characteristic of inherited human neuropathies. Nat Genet 1995; 11: 281–286.

Meyer zu Horste G, Prukop T, Liebetanz D, Mobius W, Nave KA, Sereda MW. Antiprogesterone therapy uncouples axonal loss from demyelination in a transgenic rat model of CMT1A neuropathy. Ann Neurol 2007; 61: 61–72.

Mogyoros I, Kiernan MC, Burke D. Strength-duration properties of human peripheral nerve. Brain 1996; 119 (Pt 2): 439–447.

Mogyoros I, Lin CS, Kuwabara S, Cappelen-Smith C, Burke D. Strength-duration properties and their voltage dependence as measures of a threshold conductance at the node of Ranvier of single motor axons. Muscle Nerve 2000; 23: 1719–1726.

Moldovan M, Alvarez S, Krarup C. Motor axon excitability during Wallerian degeneration. Brain 2009a; 132: 511–523.

Moldovan M, Alvarez S, Martini R, Krarup C. Investigation of ion channel abnormalities in P0-deficient knockout mice by threshold-tracking. J Neurol 2008; 255: 13.

Moldovan M, Alvarez S, Pinchenko V, Cillius F, Martini R, Krarup C. Abnormal peripheral nerve excitability in mice deficient of the myelin protein P0. PNS meeting 2009, Wurzburg Germany; 2009b.

Moldovan M, Krarup C. Mechanisms of hyperpolarization in regenerated mature motor axons in cat. J Physiol 2004; 560: 807–819.

Moldovan M, Krarup C. Evaluation of Na(+)/K(+) pump function following repetitive activity in mouse peripheral nerve. J Neurosci Methods 2006; 155: 161–171.

Moldovan M, Krarup C. Internodal function in normal and regenerated mammalian axons. Acta Physiol 2007; 189: 191–200.

Mori A, Nodera H, Shibuta Y, Okita T, Bostock H, Kaji R. Threshold-dependent effects on peripheral nerve in vivo excitability properties in the rat. Neurosci Lett 2010; 468: 248–253.

Nakata M, Baba H, Kanai K, Hoshi T, Sawai S, Hattori T, et al. Changes in Na(+) channel expression and nodal persistent Na(+) currents associated with peripheral nerve regeneration in mice. Muscle Nerve 2008; 37: 721–730.

Nave KA, Sereda MW, Ehrenreich H. Mechanisms of disease: inherited demyelinating neuropathies–from basic to clinical research. Nat Clin Pract Neurol 2007; 3: 453–464.

Nodera H, Bostock H, Kuwabara S, Sakamoto T, Asanuma K, Jia-Ying S, et al. Nerve excitability properties in Charcot-Marie-Tooth disease type 1A. Brain 2004; 127: 203–211.

Novakovic SD, Eglen RM, Hunter JC. Regulation of Na+ channel distribution in the nervous system. Trends Neurosci 2001; 24: 473–478.

Priori A, Bossi B, Ardolino G, Bertolasi L, Carpo M, Nobile-Orazio E, et al. Pathophysiological heterogeneity of conduction blocks in multifocal motor neuropathy. Brain 2005; 128: 1642–1648.

Reilly MM, Shy ME. Diagnosis and new treatments in genetic neuropathies. J Neurol Neurosurg Psychiatry 2009; 80: 1304–1314.

Samsam M, Frei R, Marziniak M, Martini R, Sommer C. Impaired sensory function in heterozygous P0 knockout mice is associated with nodal changes in sensory nerves. J Neurosci Res 2002; 67: 167–173.

Samsam M, Mi W, Wessig C, Zielasek J, Toyka KV, Coleman MP, et al. The Wlds mutation delays robust loss of motor and sensory axons in a genetic model for myelin-related axonopathy. J Neurosci 2003; 23: 2833–2839.

Sawai S, Kanai K, Nakata M, Hiraga A, Misawa S, Isose S, et al. Changes in excitability properties associated with axonal regeneration in human neuropathy and mouse Wallerian degeneration. Clin Neurophysiol 2008; 119: 1097–1105.

Schmid CD, Stienekemeier M, Oehen S, Bootz F, Zielasek J, Gold R, et al. Immune deficiency in mouse models for inherited peripheral neuropathies leads to improved myelin maintenance. J Neurosci 2000; 20: 729–735.

Schwarz JR, Glassmeier G, Cooper EC, Kao TC, Nodera H, Tabuena D, et al. KCNQ channels mediate IKs, a slow K+ current regulating excitability in the rat node of Ranvier. J Physiol 2006; 573: 17–34.

Sereda MW, Meyer zu HG, Suter U, Uzma N, Nave KA. Therapeutic administration of progesterone antagonist in a model of Charcot-Marie-Tooth disease (CMT-1A). Nat Med 2003; 9: 1533–1537.

Shapiro L, Doyle JP, Hensley P, Colman DR, Hendrickson WA. Crystal structure of the extracellular domain from P0, the major structural protein of peripheral nerve myelin. Neuron 1996; 17: 435–449.

Sleeper AA, Cummins TR, Dib-Hajj SD, Hormuzdiar W, Tyrrell L, Waxman SG, et al. Changes in expression of two

tetrodotoxin-resistant sodium channels and their currents in dorsal root ganglion neurons after sciatic nerve injury but not rhizotomy. J Neurosci 2000; 20: 7279–7289.

Sung JY, Kuwabara S, Kaji R, Ogawara K, Mori M, Kanai K, et al. Threshold electrotonus in chronic inflammatory demyelinating polyneuropathy: correlation with clinical profiles. Muscle Nerve 2004; 29: 28–37.

Thakor DK, Lin A, Matsuka Y, Meyer EM, Ruangsri S, Nishimura I, et al. Increased peripheral nerve excitability and local NaV1.8 mRNA up-regulation in painful neuropathy. Mol Pain 2009; 5: 14.

Tomlinson S, Burke D, Hanna M, Koltzenburg M, Bostock H. In vivo assessment of HCN channel current (I(h)) in human motor axons. Muscle Nerve 2010; 41: 247–256.

Ulzheimer JC, Peles E, Levinson SR, Martini R. Altered expression of ion channel isoforms at the node of Ranvier in P0-deficient myelin mutants. Mol Cell Neurosci 2004; 25: 83–94.

Warner LE, Hilz MJ, Appel SH, Killian JM, Kolodry EH, Karpati G, et al. Clinical phenotypes of different MPZ (P0) mutations may include Charcot-Marie-Tooth type 1B, Dejerine-Sottas, and congenital hypomyelination. Neuron 1996; 17: 451–460.

Waxman SG. Do 'demyelinating' diseases involve more than myelin? Nat Med 2000; 6: 738–739.

Waxman SG. Acquired channelopathies in nerve injury and MS. Neurology 2001; 56: 1621–1627.

Waxman SG, Kocsis JD, Black JA. Type III sodium channel mRNA is expressed in embryonic but not adult spinal sensory neurons, and is reexpressed following axotomy. J Neurophysiol 1994; 72: 466–470.

Weimer LH, Podwall D. Medication-induced exacerbation of neuropathy in Charcot Marie Tooth disease. J Neurol Sci 2006; 242: 47–54.

Wrabetz L, D'Antonio M, Pennuto M, Dati G, Tinelli E, Fratta P, et al. Different intracellular pathomechanisms produce diverse Myelin Protein Zero neuropathies in transgenic mice. J Neurosci 2006; 26: 2358–2368.

Yin X, Kidd GJ, Pioro EP, McDonough J, Dutta R, Feltri ML, et al. Dysmyelinated lower motor neurons retract and regenerate dysfunctional synaptic terminals. J Neurosci 2004; 24: 3890–3898.

Zielasek J, Martini R, Suter U, Toyka KV. Neuromyotonia in mice with hereditary myelinopathies. Muscle Nerve 2000; 23: 696–701.

Zielasek J, Martini R, Toyka KV. Functional abnormalities in P0-deficient mice resemble human hereditary neuropathies linked to P0 gene mutations. Muscle Nerve 1996; 19: 946–952.